Eur Radiol (2005) 15: 2146–2156
DOI 10.1007/s00330-005-2738-5



**Giacomo Luccichenti**
**Filippo Cademartiri**
**Francesca Romana Pezzella**
**Giuseppe Runza**
**Manuel Belgrano**
**Massimo Midiri**
**Umberto Sabatini**
**Stefano Bastianello**
**Gabriel P. Krestin**

# 3D reconstruction techniques made easy: know-how and pictures

Received: 4 November 2004
Revised: 11 February 2005
Accepted: 1 March 2005
Published online: 5 April 2005


G. Luccichenti (✉) · U. Sabatini
Department of Radiology,
IRCCS Fondazione Santa Lucia,
Via Ardeatina, 306,
00179 Rome, Italy
e-mail: g.luccichenti@email.it
Tel.: +39-068-5304575
Fax: +39-068-5800461

F. Cademartiri · G. P. Krestin
Department of Radiology,
Erasmus Medical Center,
University of Rotterdam,
Rotterdam, The Netherlands

F. R. Pezzella
Department of Neurological Sciences,
University of Rome La Sapienza,
Rome, Italy

G. Runza · M. Midiri
Department of Radiology,
University of Palermo,
Palermo, Italy

M. Belgrano
Deparment of Radiology,
University of Trieste,
Trieste, Italy

S. Bastianello
Department of Neuroradiology,
Institute of Neurology,
IRCCS Fondazione C. Mondino,
University of Pavia,
Pavia, Italy

**Abstract** Three-dimensional reconstructions represent a visual-based tool for illustrating the basis of three-dimensional post-processing such as interpolation, ray-casting, segmentation, percentage classification, gradient calculation, shading and illumination. The knowledge of the optimal scanning and reconstruction parameters facilitates the use of three-dimensional reconstruction techniques in clinical practise. The aim of this article is to explain the principles of multidimensional image processing in a pictorial way and the advantages and limitations of the different possibilities of 3D visualisation.

**Keywords** Computed tomography (CT), image processing · Computed tomography (CT), three-dimensional · Images, three-dimensional · Images, processing

## Introduction

The improvement of multidetector computed tomography (MDCT), with fast and high-resolution imaging, increases the overall amount of information in terms of raw data, source images and image findings [1–3]. Between 300 and 800 images can be generated with an MDCT in a single thoracic or abdominal angiographic examination. Three-dimensional reconstruction techniques allow a condensed representation of this relevant information. They make more evident the information that is fragmented in several axial slices. In addition, they can overcome the problems caused by the standard transverse orientation such as the relationships between structure shape and orientation and scan plane. It should be emphasized that, with advances in scanners technology, an increasing part of the examination is devoted to the post-processing [1, 4]. As a consequence, three-dimensional reconstructions techniques should be considered as a part of the standard radiological examination.

The aim of this paper is to describe, through a visual-based-approach, the basics of three-dimensional reconstruction techniques. The algorithm to obtain three-dimensional reconstructions embraces two main steps: namely the data acquisition, which includes scan and image reconstruction, and the post-processing, which includes several operations that will be described below.

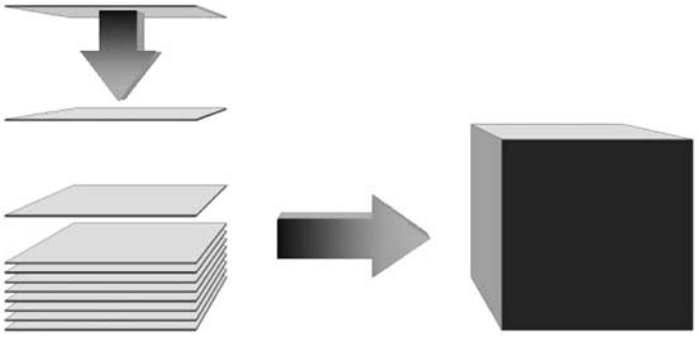

**Fig. 1** The representation of the images in a virtual three-dimensional space in their respective position produces a cube of data. Images are bidimensional and spaced. The gaps of missing data can be filled through interpolation of the values of the images. In this way, a solid cube of data is obtained. This three-dimensional cube of data is made of elementary units, which are referred as to volume elements (voxels)

## Three-dimensional reconstruction

CT generates two-dimensional pictures that are separated by gaps depending on the reconstruction increment. Filling these gaps is necessary to obtain a volume of continuous data (Fig. 1). The key to fill these gaps is interpolation. With this operation, a volume of data is obtained from several two-dimensional images. As a two-dimensional picture is formed by picture elements (pixels), a volume is formed by volume elements (voxels) (Fig. 1). Pixels and voxels can be referred as points in order to simplify the description.

### Interpolation

Interpolation estimates a missing value from known surrounding points [5]. This operation is carried out for image reconstruction in spiral CT and in three-dimensional reconstruction [6, 7]. Assume that each location has its own value. From now on, the missing value of a point that is obtained through interpolation will be referred as to the interpolated value "IV". The three most common interpolation operations are described.

With the nearest neighbour interpolation, IV is obtained from the value of the nearest point. It cannot be performed more than once. With linear interpolation, IV is obtained from the linear relationship between two known adjacent points. Yet this operation is not radial and cross-shaped artefacts might occur. Cubic convolution interpolation assigns to IV a value from four or more points. It is a radial operation and is computationally expensive. A prerequisite of this operation is that the distance between the points is small enough to assume that IV value is between these two points. If this requirement is not met, an incorrect IV is obtained. Aliasing will be discussed later in this article.

Interpolation *does not* create information. Rather, it increases the number of points with which this information is represented (Fig. 2).

### Representing a volume on a flat screen

The representation of a volume in a two-dimensional picture can be obtained by the projection of the voxels that form the volume on this surface. When projecting the volume on the flat screen, the voxels that form the volume may

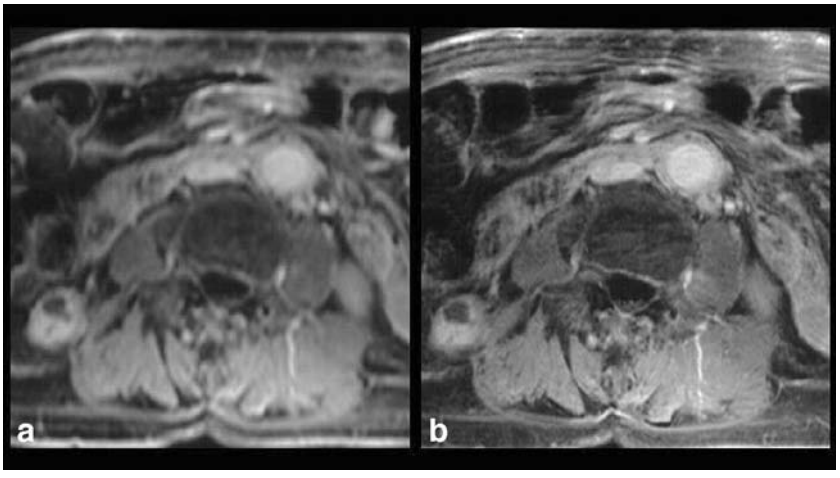


**Fig. 2** Detail of a magnetic resonance fat-saturated T1-weighted image of the abdomen. **a** Image acquisition has been performed with a 256×256 image matrix and the resulting image has been interpolated to obtain a 512×512 image matrix. **b** Image acquisition has been performed with a 512×512 image matrix. In image **b** tiny details are visible and more defined than in image **a**. The interpolation operation increases the number of pixels which represent the information. Interpolation does not provide additional information

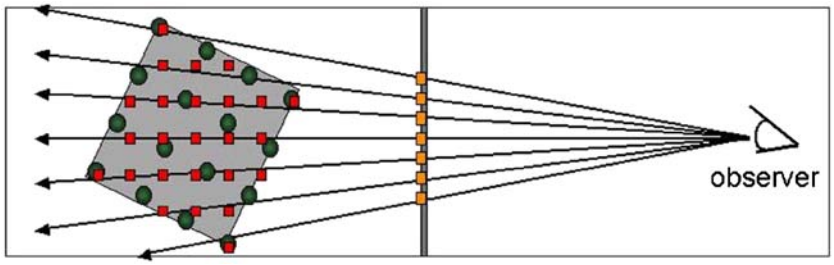


**Fig. 3** Ray casting. In ray casting, virtual lines are projected from the flat panel to the volume. The value of the pixel of the flat panel is obtained from the values of the points forming the virtual lines. A ray may not intersect the points that represent volume's voxels. The values of the missing points that form the virtual lines are obtained by interpolation from the known samples of the volume. *Red squares*: interpolated points; *yellow square*: pixel; *green circles*: points of the volume (voxels)

not correspond to the screen's pixels. One way to avoid fractional values is to perform a ray casting. With this operation projection rays are built from the screen's pixels to the volume (Fig. 3) [5, 8]. These rays may not correspond to the volume's voxels. In this case the values of the points forming the rays are obtained through interpolation. Building the rays from a hypothetic observer point of view enhances the depth perception. Projection geometry affects the visualisation of the structures (Fig. 4) [9]. The problem to represent a curved surface on a flat screen occurs similarly in cartography or in photography. In other words, optimal projection should display wide surface with minimal distortion (Fig. 5).

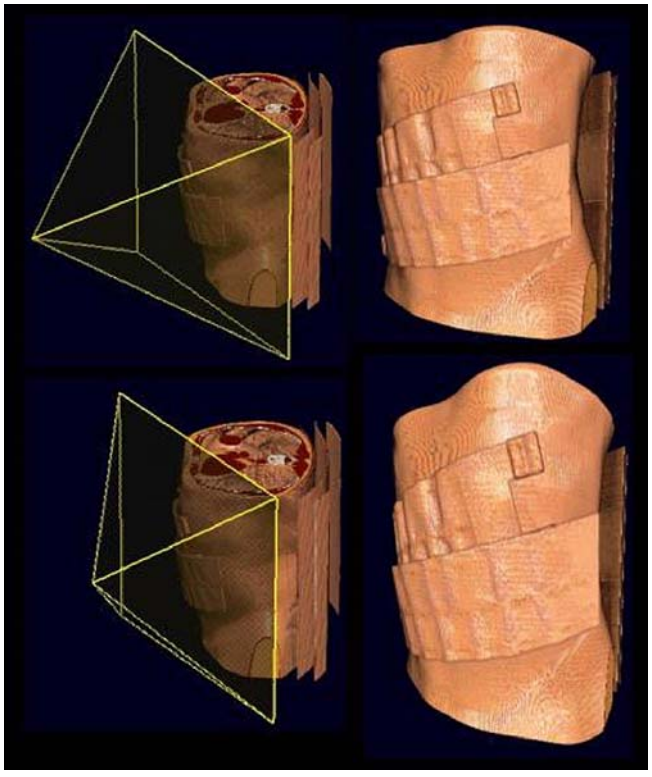

**Fig. 4** In order to enhance the depth perception, the virtual lines that are projected in ray casting are built from a location corresponding to the observer eye. From the virtual source, the rays diverge, pass through the flat screen and then through the volume. The distance between the origin of the lines and the volume enhance the depth perception, although the volume is deformed. This geometry is similar to the optic system of a camera

## Assigning a value to the screen pixel

### *Sum*

The value of the pixel from which a ray is cast can correspond to the sum of the values of the points along this ray.

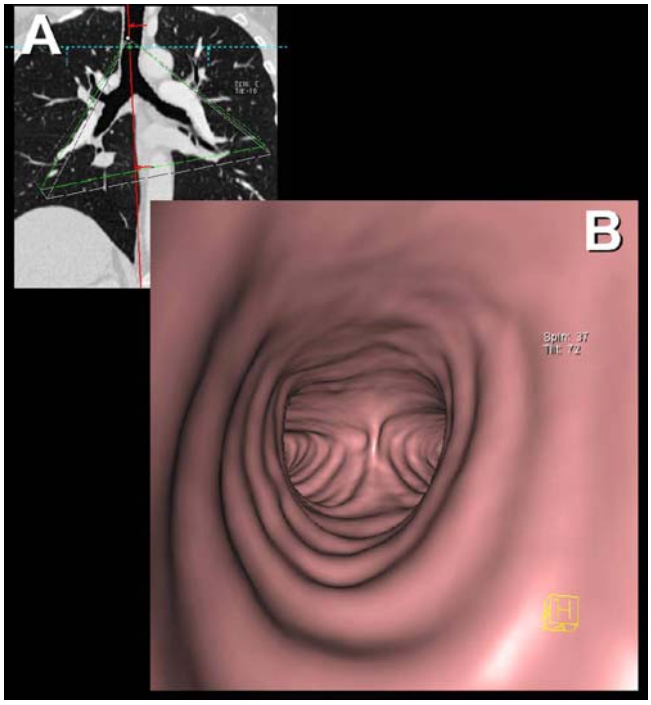


**Fig. 5** Example of virtual endoscopy (e.g. projected solid angle) with good lumen visualization of the trachea. The position of viewpoint is showed in (**a**), while the resulting image is showed in (**b**)

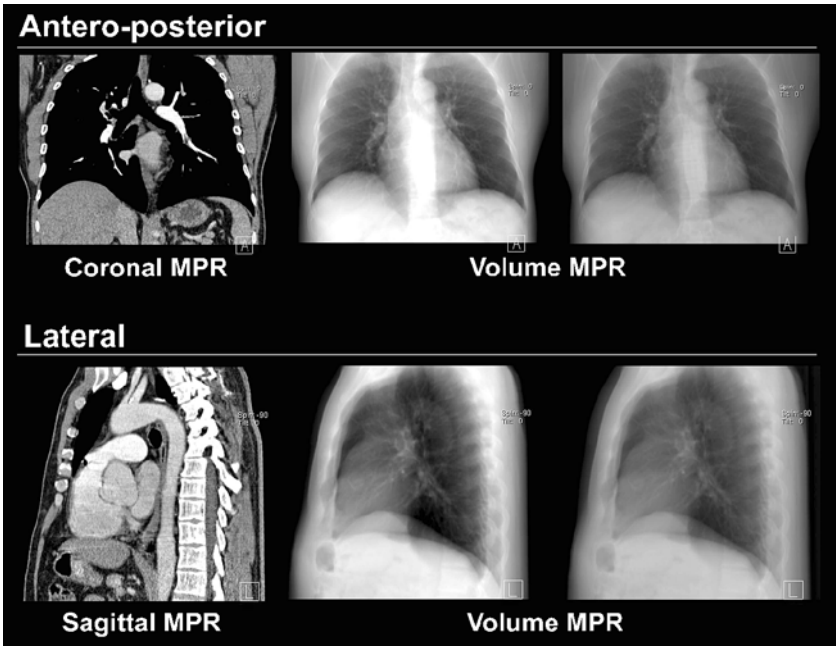


**Fig. 6** Example that shows how the sum of all voxels in the volume produces the conventional roentgenogram. In antero–posterior (upper panel) and lateral (lower panel) projections, the result of the sum of all the voxels along the observation line is a two-dimensional image, which in principle is comparable to a very thick slab multiplanar reconstruction (volume MPR)

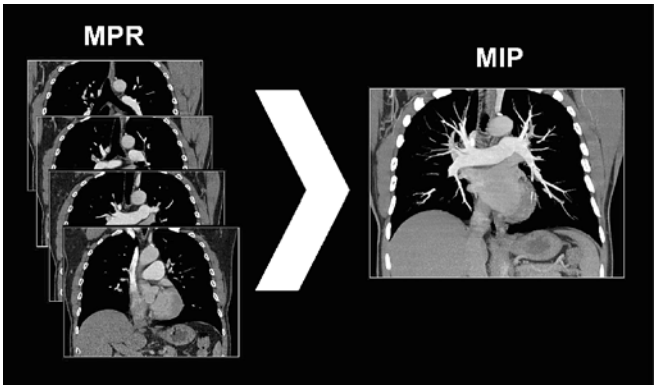


**Fig. 7** Thick slab MIP. Merging together several contiguous slices (coronal reconstruction on the left side) and projecting the highest attenuation, result in a MIP image (right side)

In this case the resulting picture is similar to a conventional roentgenogram (Fig. 6).

*Maximum intensity projection (MIP)*

If the pixel's value is equal to the interpolated voxel that has the highest value along the ray, the result is an MIP image (Fig. 7) [5]. It is possible to set the pixel value to the lowest value the ray comes across. The result is a Minimum Intensity Projection (MinIP).

One of the disadvantages of MIP is that the voxels whose value is not the highest along the ray are not represented. Hypo-intense structures within hyper-intense structures can be masked because only the material with the highest intensity along the projected ray is represented

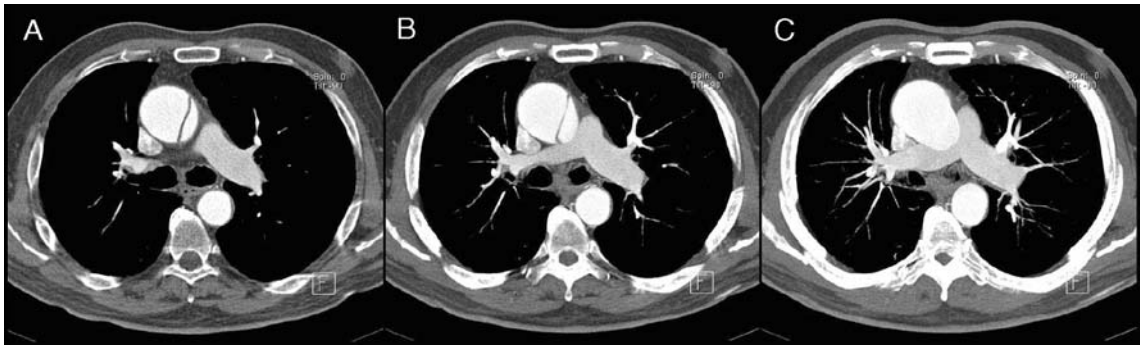


**Fig. 8** Example of pitfall of MIP. In presence of ascending aorta dissection, 1 mm thick axial images (**a**) show clearly the dissected flap. Performing a "slab axial MIP" with increasing thickness (**b**–**c**); (thickness=8 mm, 20 mm) the dissected flap progressively disappears

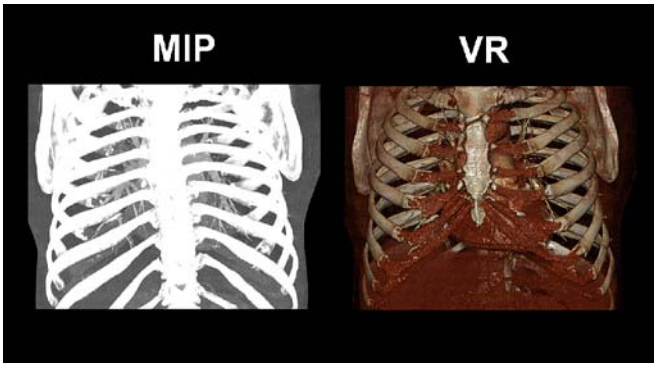


**Fig. 9** MIP and VR images. In MIP images, hyperintense structures are superimposed and the three-dimensional perception is lost

(Fig. 8). Hence, to avoid errors, axial slices must always be checked. Finally, two separated hyper-intense structures (or hyper-attenuating) along the direction of the rays appear superimposed due to the absence of the depth cue (Fig. 9) [10, 11]. Rotating the volume, in order to obtain different projection views, and analysing them as with fluoroscopic images may avoid this problem. It is also possible to trim the volume to reduce the computational costs and exclude the overlapping structures.

Attention should be addressed to the window settings, which affect structure's dimensions. In addition, due to the projective nature of the MIP image, measurements are not reliable (Fig. 10).

### *Shaded surface display (SSD)*

This technique represents the surface of a structure. In SSD the pixel's value of the final picture corresponds to the value of the point that is closest to the screen and above a selected threshold (Fig. 11). The threshold determines how much the resulting image respects actual anatomy. The SSD image does not provide any densitometric information [11]. Calcifications of vascular structures and the contrast material are represented in the same way [10]. If the threshold is not correctly selected, the stool in a virtual colonography examination is visualized as a part of the mucosa, simulating a tumour. A depth-encoded shading scale makes the closer voxel to appear brighter enhancing the depth perception.

### *Volume rendering and percentage classification*

Classification is the operation that defines how each point along the ray contributes to the pixel value on the picture (Figs. 12, 13) [5, 8, 12]. The contribution may range from 100 to 0% opacity. An opacity function curve correlates the voxel value with its opacity. The pixel value of the screen will be obtained from the contribution of the opacities of the points along the ray. Only voxels, the values of which lay within selected interval, are represented. The voxels that are outside of this interval are transparent. In CT, voxel value corresponds to the attenuation in Hounsfield Units (HU). The shape of the curve defines the visibility of the structures in keeping with their attenuation (Fig. 12, 13) [13]. The pixel value can be represented through grey- or a colour scale, which may enhance the depth perception and the densitometric information. While in SSD the pixel's value depends on the virtual distance of the volume from the screen, in VR it depends on the pixel's value enclosing densitometric information. In other words, VR provides both spatial and densitometric information (Figs. 9, 12, 13).

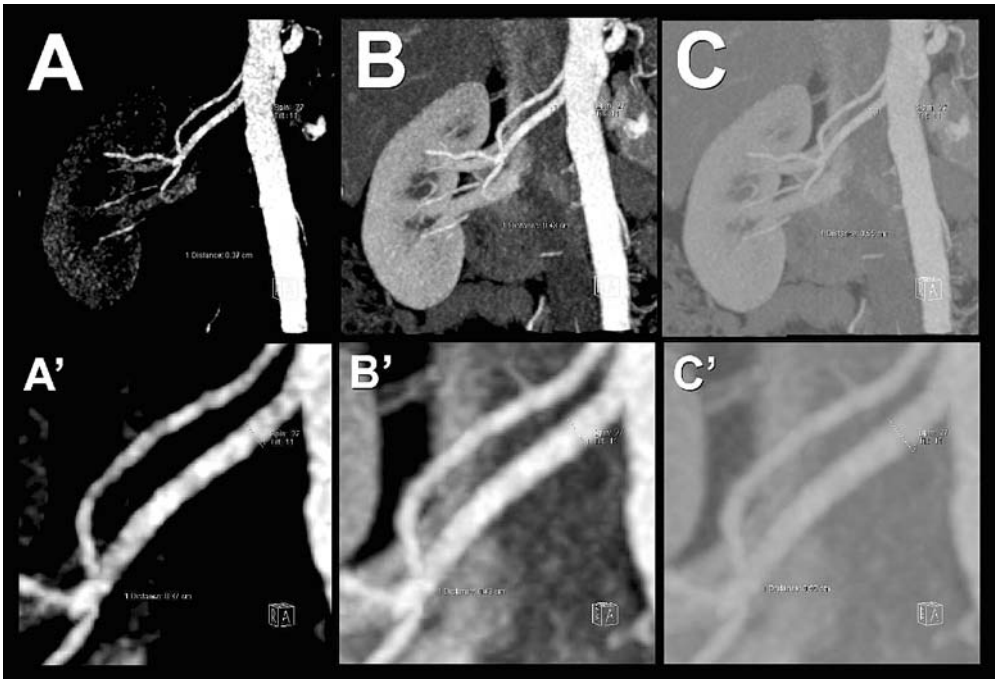


**Fig. 10** Example of how MIP settings (e.g. window settings) can affect vessel measurements. In a patient with double right renal artery, different window settings are applied: close (**a**), medium (**b**), wide (**c**). The corresponding measurement of the diameter of the main renal artery is different depending on the respective settings

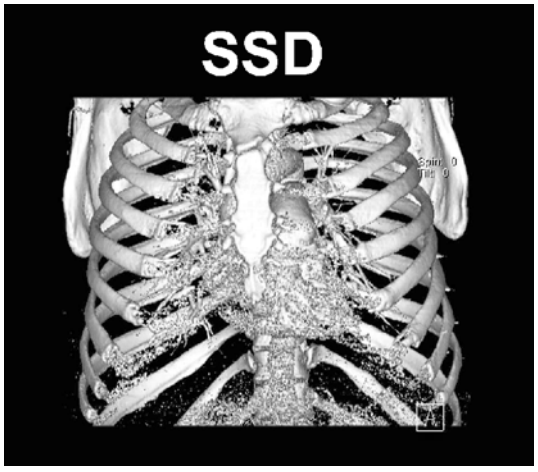


**Fig. 11** Example of volumetric Surface Shaded Display—SSD

As for MIP and SSD, measurements performed in the VR images are not reliable: the rendering and opacity function settings strongly affects visibility and dimensions of structures.

## Multiplanar reformatting (MPR)

MPR generates from native slices images laying in a different plane. The best way to understand the MPR is to figure out the above-mentioned screen lying within the volume (Fig. 14) [5]. The values of the pixels forming the reformatted plane are obtained through interpolation from the closest voxels. If more distant voxels contribute to the final picture, the result is a "thick slab". Pictures of a curved plane, lying along a vessel for instance, can be obtained in the same way (Fig. 15).

MPR is useful to assess spatial relationships of structures oriented in the scan plane. In addition, MPR allows to overcome the error of the measurement of a structure which is obliquely oriented in respect to the scan plane.

## Enhancing the depth perception

In volume rendering, surfaces are identified by estimating the gradient of variation of the voxel's values within a volume. This is particularly useful for the application of shading and illumination operations [5, 12].

Put simply, shading operations modify the "colour" of the surface according to the light intensity in the scene. Illumination operation modifies the "colour" of the surface according to the angle of incidence of a light originating from a virtual source. In addition the texture of the surface affects the light reflection. A smooth surface is supposed to reflect better than an irregular one (Fig. 16).

## Segmentation

Segmentation labels the voxel that form an object within the volume. Segmentation can be performed manually or with semi-automatic or automated software [14]. An object can be identified on the basis of morphology, density, homogeneity, its inherent structure and location within the volume [12, 15, 16]. If the object has not at least one feature allowing its identification, its segmentation will not be accurate or possibly not even feasible. Segmentation is challenging when structures or tissues with similar densities surround the object or are connected with it. Object margins can be defined by setting a threshold, manually, using morphological operations or through advanced algorithms [14, 17]. Hypodense fatty layers are useful to define margins of non-fatty structures. Vascular structures can be segmented

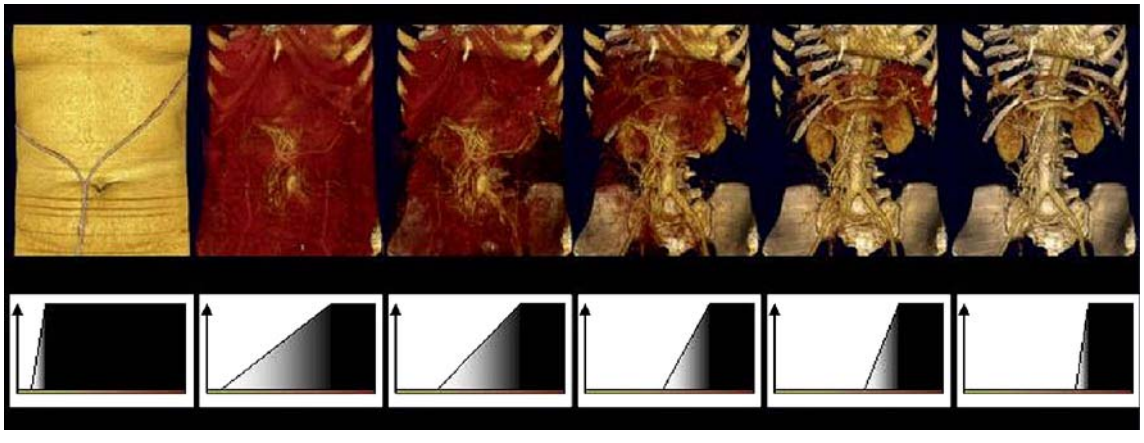

**Fig. 12** Classification. The shape of the opacity function curve defines the anatomical structures that is visualised according to the attenuation value. From left to right, the soft tissues are progressively made transparent

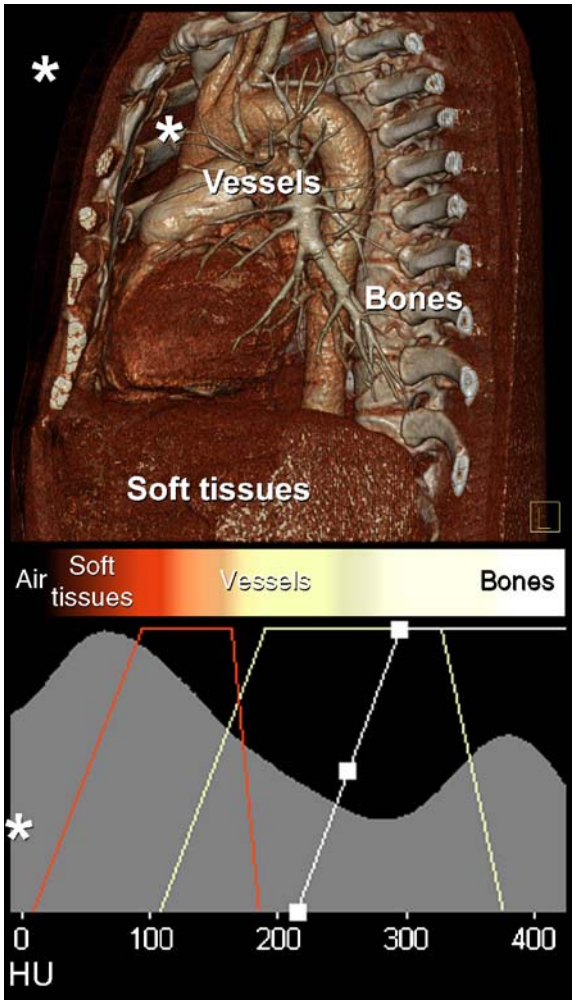


**Fig. 13** When looking at VR images, depending on the settings applied, it is possible to distinguish clearly between the different densities and tissues. In this image (upper panel) the colour/density scale (lower panel) of represented voxels goes from 0HU to +1000 HU. There are three ranges of colour partially overlapped that create a continuous range of colour and opacities from *dark red* (for soft tissues), to *dark and bright yellow* (for vessels), to *white* (for bones). Tissues and structures outside the range of opacities are completely transparent (*asterisk*) such as lung parenchyma, and surrounding air

manually or with automatic-tracking tools, using the high differential density of the vessel lumen compared to the surrounding structures. Automated path finding in virtual CT colonoscopy is made possible with similar principles. Segmentation allows an accurate assessment and volume, surface or histogram analysis of the segmented object (Fig. 17) [18, 19]. In addition, segmentation is a fundamental operation for unwrapping hollow viscera and for automated lesion detection, which is of great interest in screening programs [20–22].

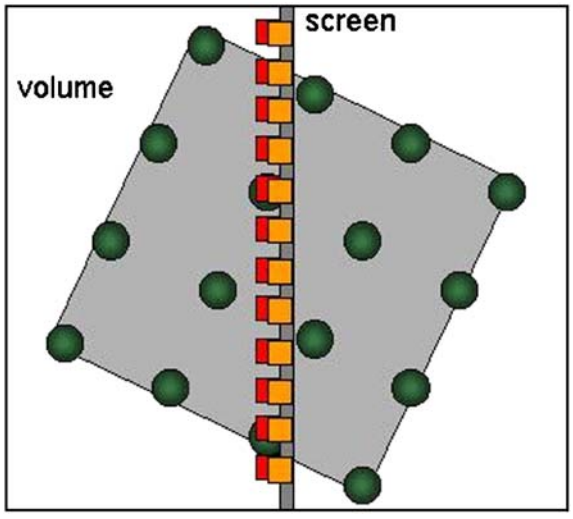


**Fig. 14** Multiplanar reformation. In multiplanar reformation, the points of the plane crossing the volume are obtained by interpolation from the known points of the volume. *Red squares*: interpolated points; *yellow square*: pixel; *green circles*: points of the volume (voxels)

## Optimizing scanning parameters for three-dimensional reconstructions

The basic concept for optimising scanning parameters for three-dimensional imaging is to obtain a small and noiseless voxel. In addition, voxel size shall be small enough for adequate representation of the studied structures. In order to optimise scanning parameters, four factors should be considered:

1. Spatial resolution, which represents the capability to discern two points. Cross-sectional images with low spatial resolution produce 3D images that look blurred (Fig. 18).
2. Contrast resolution, which can be described with the contrast to noise ratio (CNR), represents the capability to discern two densities with a given background noise.
3. Aliasing, which is due to an insufficient sampling frequency with respect to the frequency of the sampled signal. Aliasing may manifest with stair-step artifacts of oblique oriented structures in the *z*-axis or as additive noise (Fig. 19) [23–25]. High reconstruction increment generates aliasing.
4. Artifacts, such as those due to the interpolation geometry in CT reconstruction associated with high contrast interfaces, which are obliquely oriented, generating rotational artifact and object deformation [24–26]. These artifacts are prominent with high pitch.

Factors affecting cross-sectional images also affect three-dimensional reconstructions. Scanning parameters and reconstruction operations affect spatial and contrast resolution,

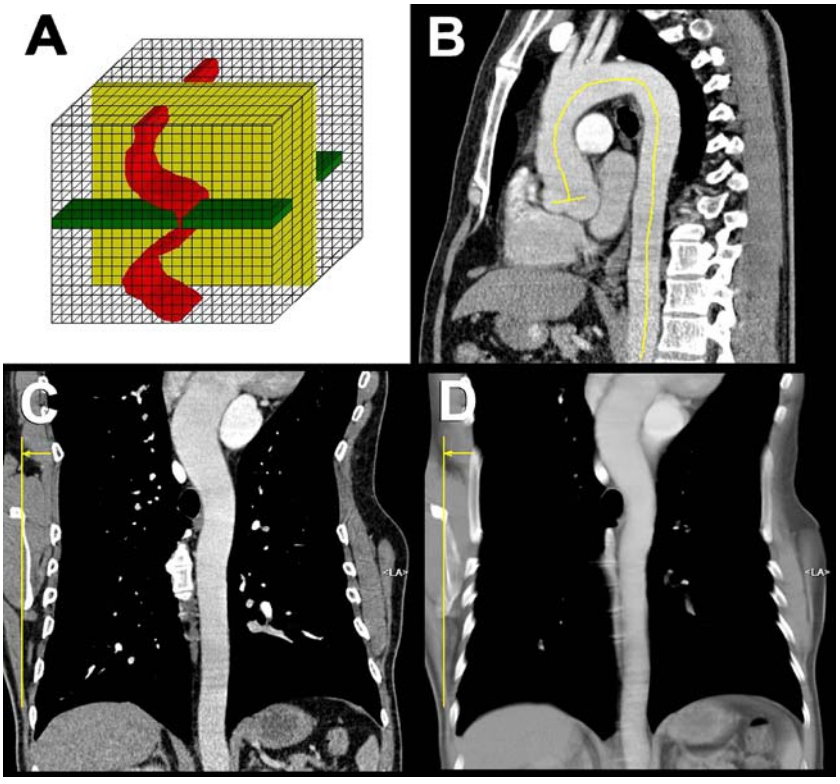


**Fig. 15** Curved reformatted images. Images in curved planes can be generated by calculating the value of the pixel by interpolation form the voxel's values of the volume (**a**) *red plane*. In **b**, a thoracic aorta is segmented with a curved central lumen line in order to obtain curved projections of the entire lumen in one plane (**c**). On curved images it is also possible to use thick slabs (**d**)

particularly in the *z*-axis [27–29]. Among parameters that can be set by the operator, collimation, pitch and reconstruction increment are particularly important.

Narrow collimations increase image noise and spatial resolution and vice versa [25, 30]. Since 3D images display information enclosed in axial slices, exceeding in collimation width produces 3D images that look blurred. Collimation should be set according to the object size and the helical pitch [30, 31]. In addition, wide collimations generate partial volume effects due to the averaging of the densities within the volume.

High pitch entails object distortion along the *z*-axis, aliasing, and a rotation artifact [23, 24, 26, 32]. For large volume coverage a thin collimation and a high table feed should be preferred rather than the opposite option, because higher longitudinal resolution is obtained [30]. While ex-

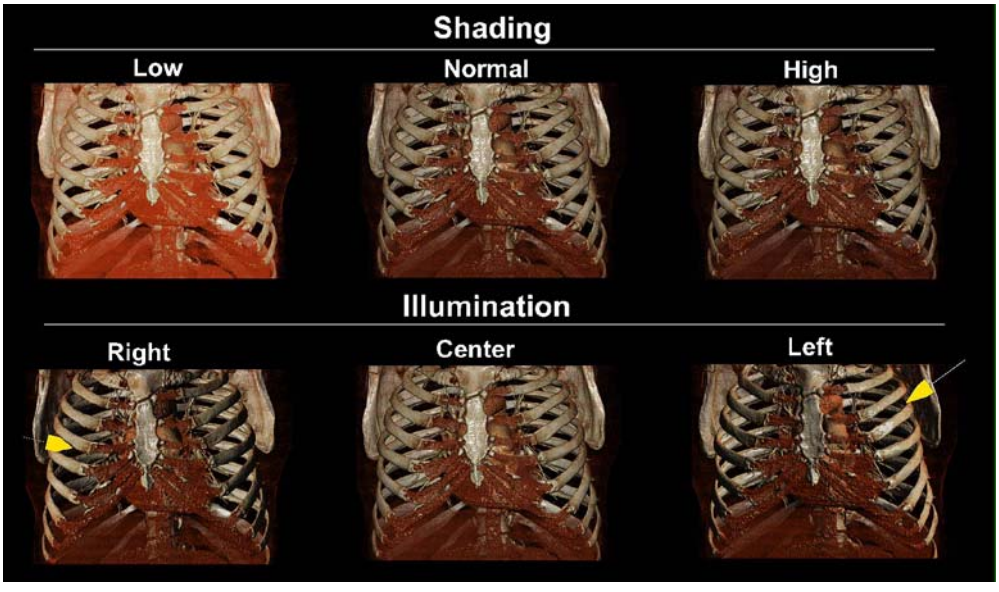


**Fig. 16** Shading and illumination. Shading modify the colour of the phantom according to the virtual distance from the observer, to the texture and the features of the surface. Illumination modify the colour of the phantom according to the direction and the features of the virtual source of light. Shadows are generated accordingly. The respective effect of different shading levels (*upper panel*) and illumination orientations (*lower panel*) are displayed

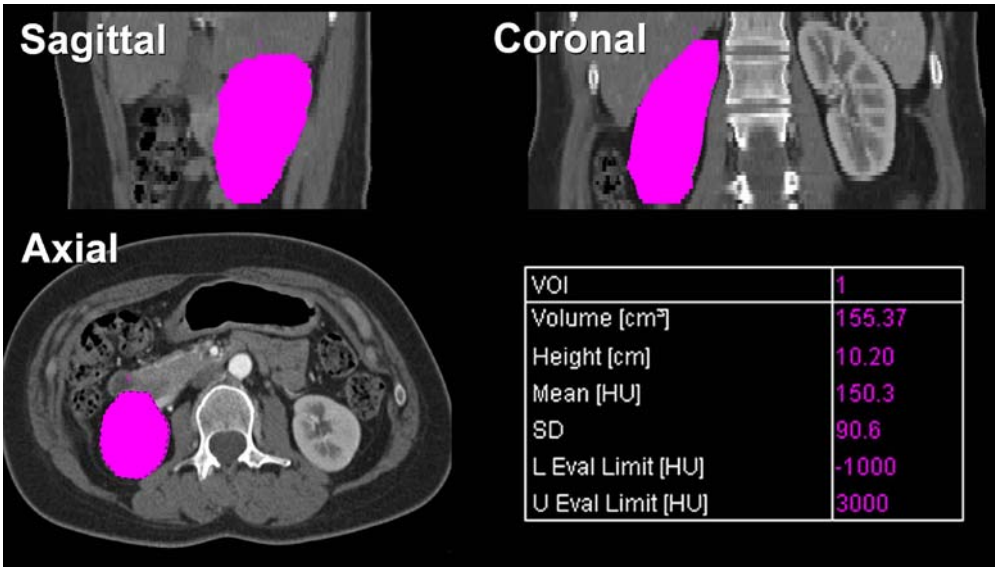


**Fig. 17** Segmentation. The use of segmentation tools allows measurement of the exact volume of organs and calculation of the mean attenuation such as, in this case, with a right kidney

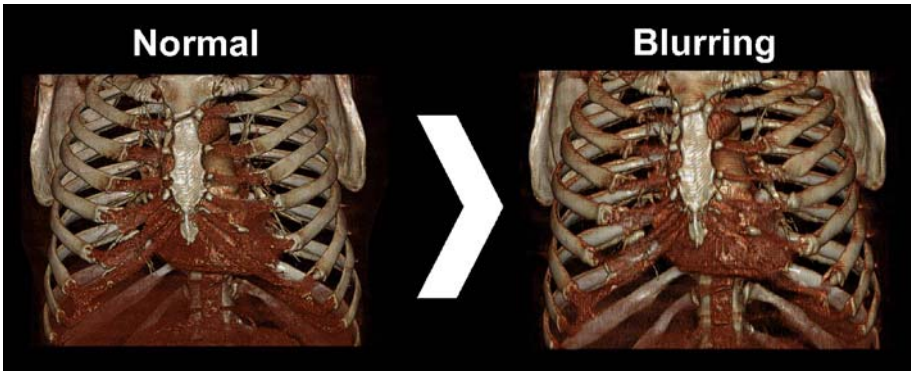


**Fig. 18** Three-dimensional image blurring. Using thicker slices to perform three-dimensional VR results in a blurring of the images

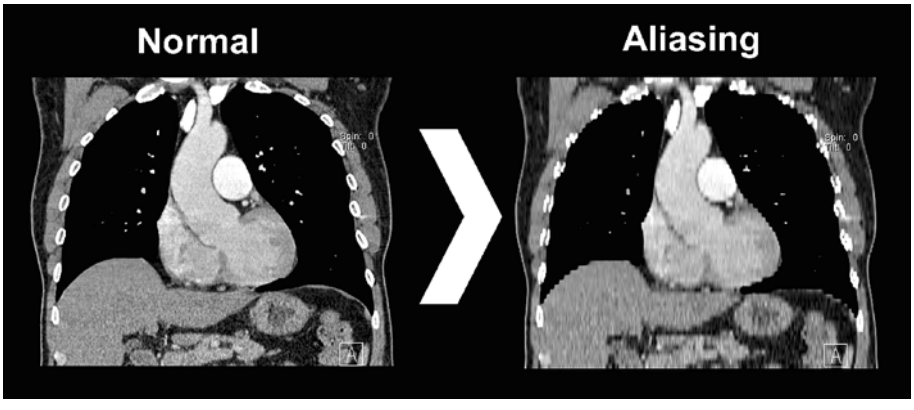


**Fig. 19** Aliasing. An insufficient sampling frequency results in image aliasing. The example shows a coronal image of the thorax that was reconstructed from a dataset with slice thickness and increment of 1 mm/1 mm (*left side*), and the same image generated with a dataset with slice thickness and increment of 3 mm/3 mm (*right side*)

tensive volume coverage with high-resolution is limited in SLCT due to tube's heating, MSCT solve this problem [33].

The reconstruction increment (RI) is responsible for the gaps between the images. Narrow RI increases spatial and contrast resolution, minimizing aliasing [6, 27, 30, 34, 35]. A drawback of overlapping slices is the increased number of images. On the other hand, high RI generate aliasing [26].


**Fig. 20** Convolution kernels. Low filtering results in smooth images but with sub-optimal depiction of the lung parenchyma (**a**). High filters, even with increased noise, provide a better visualization of the lung parenchyma (**b**). A further application of higher filters is the study of coronary stents. From **c** to **e** increasing filters improve the visualization of coronary lumen in a stent of the right coronary artery

Effective slice width is the thickness of the reconstructed slice in MSCT and may differ from the thickness of the detector. Given an effective slice width, thinner collimations provide higher image quality but enhance artifacts [24].

Convolution kernels are applied before back-projection of raw data for image reconstruction. Alternatively filters can be applied in two-dimensional images [36]. Sharp kernels and filters are used to enhance the edges of high-contrast structures (lung parenchyma or bone). Yet, in this instance image noise is amplified (Fig. 20). Smooth kernels or filters enhance CNR reducing image noise.

## References


1. Mahesh M (2002) Search for isotropic resolution in CT from conventional through multiple-row detector. Radiographics 22:949–962
2. Ferretti GR, Bricault I, Coulomb M (2001) Virtual tools for imaging of the thorax. Eur Respir J 18:381–392
3. Grenier PA, Beigelman-Aubry C, Fetita C et al. (2002) New frontiers in CT imaging of airway disease. Eur Radiol 12:1022–1044
4. van Ooijen PM, Ho KY, Dorgelo J, Oudkerk M (2003) Coronary artery imaging with multidetector CT: visualization issues. Radiographics 23:e16
5. Lichtenbelt B, Crane R, Naqvi S (1998) Introduction to volume rendering. Prentice Hall PTR, Upper Saddle River, NJ 07458
6. Polacin A, Kalender WA, Marchal G (1992) Evaluation of section sensitivity profiles and image noise in spiral CT. Radiology 185:29–35
7. Kalender WA, Seissler W, Klotz E, Vock P (1990) Spiral volumetric CT with single-breath-hold technique, continuous transport, and continuous scanner rotation. Radiology 176:181–183
8. Calhoun PS, Kuszyk BS, Heath DG et al. (1999) Three-dimensional volume rendering of spiral CT data: theory and method. Radiographics 19:745–764
9. Paik DS, Beaulieu CF, Jeffrey RB Jr et al. (2000) Visualization modes for CT colonography using cylindrical and planar map projections. J Comput Assist Tomogr 24:179–188
10. Semba CP, Rubin GD, Dake MD (1994) Three-dimensional spiral CT angiography of the abdomen. Semin Ultrasound CT MR 15:133–138
11. Sato Y, Shiraga N, Nakajima S et al. (1998) Local maximum intensity projection (LMIP): a new rendering method for vascular visualization. J Comput Assist Tomogr 22:912–917
12. Udupa JK (1999) Three-dimensional visualization and analysis methodologies: a current perspective. Radiographics 19:783–806
13. Fishman EK, Magid D, Ney DR et al. (1991) Three-dimensional imaging. Radiology 181:321–337
14. Hohne KH, Hanson WA (1992) Interactive 3D segmentation of MRI and CT volumes using morphological operations. J Comput Assist Tomogr 16:285-294

15. Masutani Y, MacMahon H, Doi K (2001) Automated segmentation and visualization of the pulmonary vascular tree in spiral CT angiography: an anatomy-oriented approach based on three-dimensional image analysis. J Comput Assist Tomogr 25:587–597
16. Clarke LP, Velthuizen RP, Camacho MA et al. (1995) MRI segmentation: methods and applications. Magn Reson Imaging 13:343–368
17. Paik DS, Beaulieu CF, Jeffrey RB et al. (1998) Automated flight path planning for virtual endoscopy. Med Phys 25:629–637
18. Frericks BB, Caldarone FC, Nashan B et al. (2004) 3D CT modeling of hepatic vessel architecture and volume calculation in living donated liver transplantation. Eur Radiol 14:326–333
19. Luccichenti G, Cademartiri F, Cobelli R, Pavone P (2003) Assessment of organ volume with different techniques using a living liver model. Eur Radiol 13:1286–1290
20. Summers RM, Beaulieu CF, Pusanik LM et al. (2000) Automated polyp detector for CT colonography: feasibility study. Radiology 216:284–290
21. Zhang Z, Wang G, Brown BP et al. (2000) Fast algorithm for soft straightening of the colon. Acad Radiol 7:142–148
22. Masutani Y, Yoshida H, MacEneaney PM, Dachman AH (2001) Automated segmentation of colonic walls for computerized detection of polyps in CT colonography. J Comput Assist Tomogr 25:629–638
23. Yen SY, Rubin GD, Napel S (1999) Spatially varying longitudinal aliasing and resolution in spiral computed tomography. Med Phys 26:2617–2625
24. Fleischmann D, Rubin GD, Paik DS et al. (2000) Stair-step artifacts with single versus multiple detector-row helical CT. Radiology 216:185–196
25. Hopper KD, Pierantozzi D, Potok PS et al. (1996) The quality of 3D reconstructions from 1.0 and 1.5 pitch helical and conventional CT. J Comput Assist Tomogr 20:841–847
26. Wang G, Vannier MW (1994) Stair-step artifacts in three-dimensional helical CT: an experimental study. Radiology 191:79–83
27. Kalender WA, Polacin A, Suss C (1994) A comparison of conventional and spiral CT: an experimental study on the detection of spherical lesions. J Comput Assist Tomogr 18:167–176
28. Brink JA, Heiken JP, Balfe DM et al. (1992) Spiral CT: decreased spatial resolution in vivo due to broadening of section-sensitivity profile. Radiology 185:469–474
29. Khan MF, Herzog C, Ackermann H et al. (2004) Virtual endoscopy of the tracheo–bronchial system: sub-millimeter collimation with the 16-row multidetector scanner. Eur Radiol 14:1400–1405
30. Hu H, Fox SH (1996) The effect of helical pitch and beam collimation on the lesion contrast and slice profile in helical CT imaging. Med Phys 23:1943–1954
31. Beaulieu CF, Napel S, Daniel BL et al. (1998) Detection of colonic polyps in a phantom model: implications for virtual colonoscopy data acquisition. J Comput Assist Tomogr 22:656–663
32. Hu H (1999) Multi-slice helical CT: scan and reconstruction. Med Phys 26:5–18
33. Wang G, Vannier MW (1996) Maximum volume coverage in spiral computed tomography scanning. Acad Radiol 3:423–428
34. Hopper KD, Iyriboz TA, Mahraj RP et al. (1998) CT bronchoscopy: optimization of imaging parameters. Radiology 209:872–877
35. Brink JA (1995) Technical aspects of helical (spiral) CT. Radiol Clin North Am 33:825–841
36. Wildberger JM, Mahnken AM, Flohr T et al. (2003) Spatial domain image filtering in computed tomography: feasibility study in pulmonary embolism. Eur Radiol 13:717–723